Journal of Fluorine Chemistry 130 (2009) 158–161

Contents lists available at ScienceDirect

Journal of Fluorine Chemistry

journal homepage: www.elsevier.com/locate/fluor

Synthesis and upconversion luminescence properties of YF_3:Yb^{3+}/Tm^{3+} octahedral nanocrystals

Guofeng Wang [a], Weiping Qin [a,*], Guodong Wei [a], Lili Wang [a,b], Peifen Zhu [a], Ryongjin Kim [a], Daisheng Zhang [a,c], Fuheng Ding [a], Kezhi Zheng [a]

[a] State Key Laboratory on Integrated Optoelectronics, College of Electronic Science and Engineering, Jilin University, Changchun 130012, PR China
[b] School of Basic Sciences, Changchun University of technology, Changchun 130012, China
[c] College of Physics, Beihua University, Jilin 132011, PR China

ARTICLE INFO

Article history:
Received 14 August 2008
Received in revised form 18 September 2008
Accepted 19 September 2008
Available online 30 September 2008

PACS:
78.66.J
82.80.C

Keywords:
Nanocrystals
Rare earth
Upconversion
Luminescence

ABSTRACT

YF_3:Yb^{3+}(20%)/Tm^{3+}(2%) octahedral nanocrystals were synthesized by a microemulsion method with NH_4HF_2. Pumped with a 980-nm diode laser, the nanocrystals emitted weak blue and intense ultraviolet light. Especially, unusual $^3P_2 \rightarrow {}^3H_6$ (~265 nm) and $^3P_2 \rightarrow {}^3F_4$ (~309 nm) emissions, coming from a five-photon excitation process, were observed. The emissions from $^1D_2$ and $^1I_6$ were much stronger than those from $^1G_4$ and $^3H_4$. The upconversion mechanism was discussed in detail.

1. Introduction

Recently, frequency upconversion (UC) from infrared (IR) to visible/ultraviolet (UV) in rare earth doped solids has attracted much attention due to its potential applications in detection of infrared radiation, optical storage, color display, UC lasers, biosensor, and so on [1–6]. Most of these applications have been achieved with the help of fluorides due to their low phonon energy and high quantum efficiencies as luminescent hosts. Especially, Yb^{3+}/Tm^{3+}-codoped YF_3 nanocrystals have been widely studied because not only YF_3 is an important host crystal, but also Tm^{3+} has stable excited level suitable for emitting blue and UV UC luminescence simultaneously [7–12]. For example, our group has reported enhanced UV UC in Yb^{3+}/Tm^{3+}-codoped YF_3 nanocrystals [13] and Chen's group reported intense UV UC luminescence from Yb^{3+}/Tm^{3+}-codoped YF_3 nanocrystals embedded glass ceramic [14]. Despite the fact that UV UC emissions have been widely investigated and some novel spectral phenomena have been reported, the study of new approaches to obtain efficient UV luminescence as well as the mechanism of the enhancement is still a challenge for the development of short-wavelength solid-state lasers.

In this paper, YF_3:Yb^{3+}(20%)/Tm^{3+}(2%) octahedral nanocrystals were synthesized by microemulsion method. Under 980-nm excitation, the nanocrystals emitted weak blue and intense UV light. The luminescence intensity of $^1I_6 \rightarrow {}^3H_6$ is ~3 times stronger than that of $^1G_4 \rightarrow {}^3H_6$. Even compared to that from the Yb^{3+}/Tm^{3+}-codoped YF_3 nanocrystals reported previously [13], the emission peak ($^1I_6 \rightarrow {}^3H_6$) is also much higher. The UC mechanisms were analyzed in detail.

2. Results and discussion

The crystal structure was analyzed by a Rigaku RU-200b X-ray powder diffractometer (XRD), as shown in Fig. 1a. All the diffraction peaks can be indexed to the pure orthorhombic YF_3 (ICPDS 74-0911). No other impurity peaks were detected. The

* Corresponding author. Tel.: +86 431 85168240 8325; fax: +86 431 85168240 8325.
E-mail address: wpqin@jlu.edu.cn (W. Qin).

0022-1139/$ – see front matter © 2008 Elsevier B.V. All rights reserved.
doi:10.1016/j.jfluchem.2008.09.009

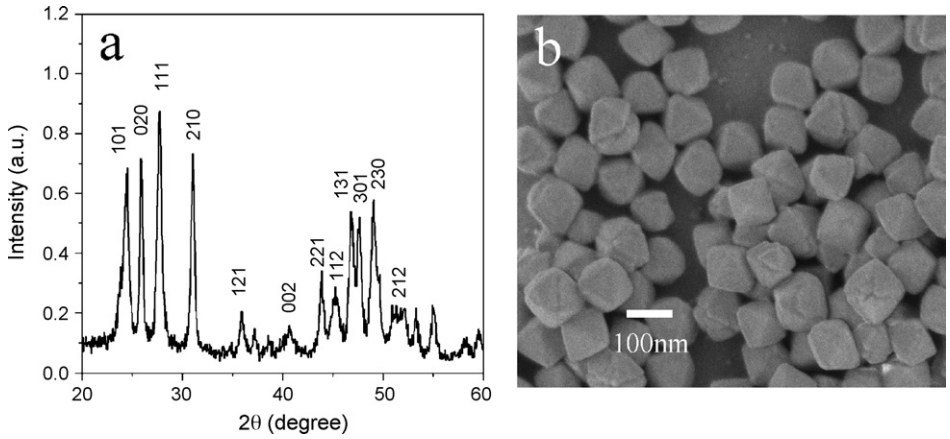

Fig. 1. XRD pattern (a) and SEM image (b) of YF_3:Yb^{3+}(20%)/Tm^{3+}(2%) nanocrystals.

morphology of the product was characterized by scanning electron microscope (SEM), as shown in Fig. 1b. Plenty of almost uniform and regular octahedral with an average length of about 100 nm can be seen in Fig. 1b.

Fig. 2 shows the UC luminescence spectrum of YF_3:Yb^{3+}(20%)/Tm^{3+}(2%) nanocrystals under 980-nm excitation. The UV, blue, red, and near infrared emissions were observed. These spectral peaks correspond to the following transitions: $^3P_2 \rightarrow {}^3H_6$ (~265 nm), $^1I_6 \rightarrow {}^3H_6$ (~291 nm), $^3P_2 \rightarrow {}^3F_4$ (~309 nm), $^1I_6 \rightarrow {}^3F_4$ (~346 nm), $^1D_2 \rightarrow {}^3H_6$ (~362 nm), $^1D_2 \rightarrow {}^3F_4$ (~457 nm), $^1G_4 \rightarrow {}^3H_6$ (~477 nm), $^1D_2 \rightarrow {}^3H_5$ (~510 nm), $^1D_2 \rightarrow {}^3H_4$ (~580 nm), $^1G_4 \rightarrow {}^3F_4$ (~642 nm), $^3F_3 \rightarrow {}^3H_6$ (~690 nm), and $^3H_4 \rightarrow {}^3H_6$ (~804 nm). Obviously, the $^1I_6 \rightarrow {}^3H_6$, $^1I_6 \rightarrow {}^3F_4$, $^1D_2 \rightarrow {}^3H_6$, and $^1D_2 \rightarrow {}^3F_4$ transitions were much stronger than the $^1G_4 \rightarrow {}^3H_6$ transition. Here, we used a PMT (Hamamatsu R928) as the detector, and therefore the relative intensity ratio of the two emissions reflects the relative ratio of them in photons/second.

A careful analysis of the luminescence dynamics of YF_3:Yb^{3+}(20%)/Tm^{3+}(2%) nanocrystals can reveal the physical mechanism behind the strong UV UC luminescence. To investigate the fundamental UC mechanism of sample, the pumping power dependence of the fluorescent intensity was investigated. For an unsaturated UC process, the emission intensity is proportional to the n-th power of the excitation intensity, and the integer n is the number of the laser photons absorbed per upconverted photon emitted [15]. Fig. 3 shows the double logarithmic plots of the emission intensity as a function of excitation power for the $^3P_2 \rightarrow {}^3H_6$, $^1I_6 \rightarrow {}^3H_6$, $^1D_2 \rightarrow {}^3H_6$, $^1G_4 \rightarrow {}^3H_6$, and $^3H_4 \rightarrow {}^3H_6$ emissions. When the excitation power is less than 0.1 W, the slopes of the linear fittings are 4.79 for $^1I_6 \rightarrow {}^3H_6$, 3.71 for $^1D_2 \rightarrow {}^3H_6$, 2.87 for $^1G_4 \rightarrow {}^3H_6$, and 1.90 for $^3H_4 \rightarrow {}^3H_6$, indicating that five, four, three, and two pumping photons are required to populate the $^1I_6$, $^1D_2$, $^1G_4$, and $^3H_4$ emitting levels, respectively. The experimental results are different from those in Ref. [16]. In this reference, the authors believed that six and five pumping photons were required to populate the $^1I_6$ and $^1D_2$ levels, respectively. When the excitation power exceeds 0.1 W, the corresponding slopes of the linear fittings reduce to 2.62, 1.98, 1.82, and 1.06 respectively. Pollnau attributed

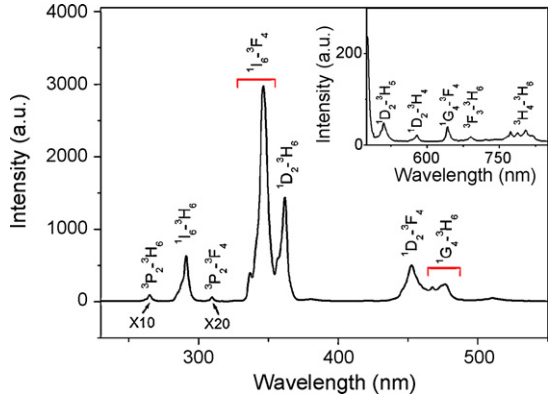

Fig. 2. UC luminescence spectrum of YF_3:Yb^{3+}(20%)/Tm^{3+}(2%) nanocrystals under 980-nm excitation (320 W cm^{-2}). Inset: magnification of the spectrum in the range of 475–850 nm.

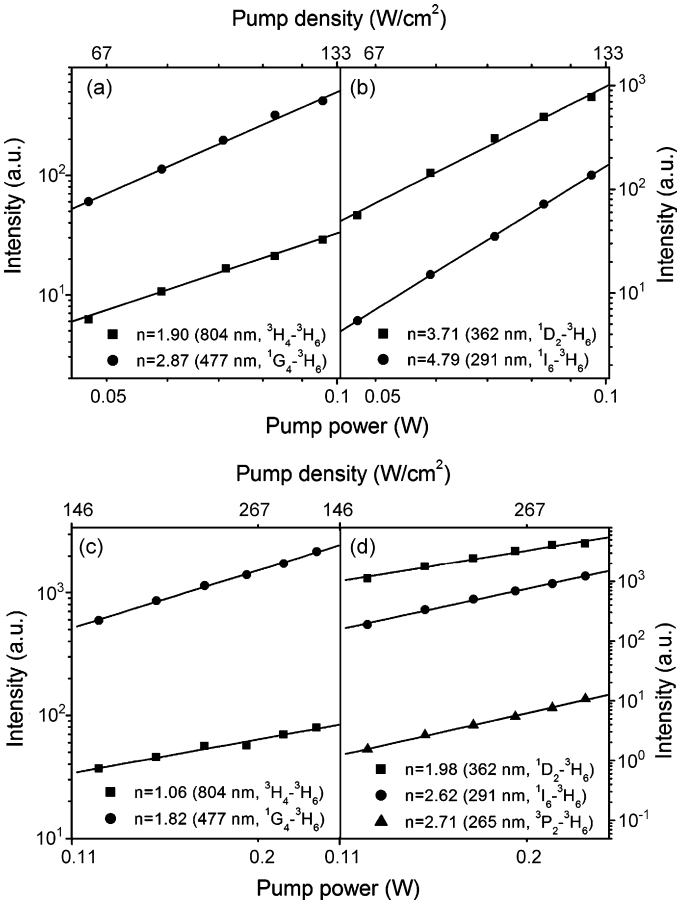

Fig. 3. Plots (log–log) of emission intensity versus excitation power.

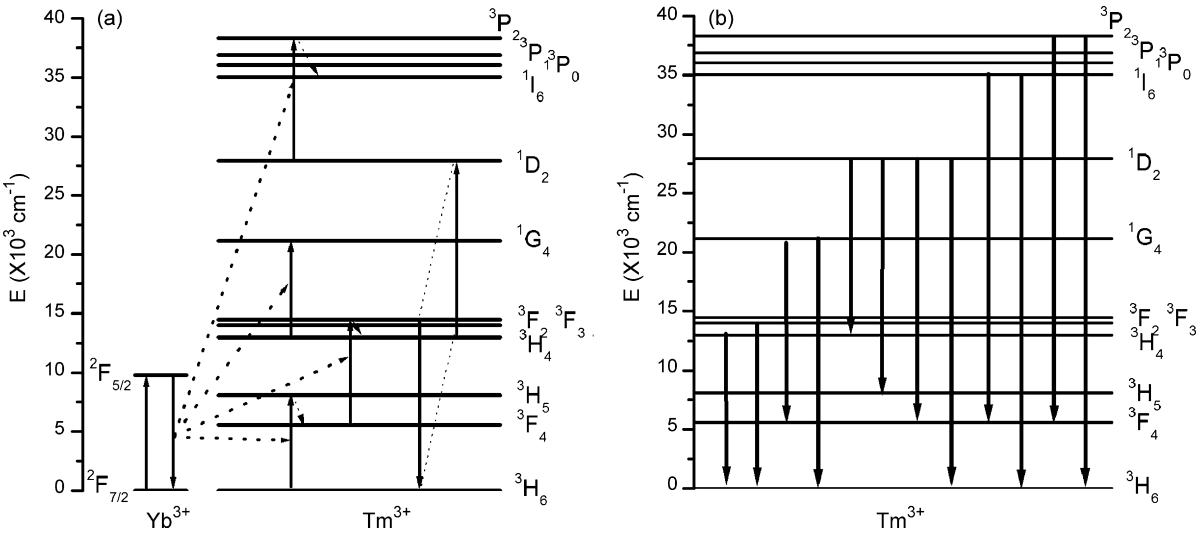

Fig. 4. Population (a) and photoluminescence processes (b) in YF_3:Yb^{3+}(20%)/Tm^{3+}(2%) nanocrystals.

the decrease of n to the competition between linear decay and UC processes for the depletion of the intermediate excited states [15]. It is noted that the $^3P_2 \rightarrow {}^3H_6$ emission was hardly observed when the excitation power is less than 0.1 W.

Fig. 4 shows the population and photoluminescence processes in YF_3:Yb^{3+}(20%)/Tm^{3+}(2%) nanocrystals [14]. The pump light excites only the Yb^{3+} ions, and three successive energy transfers from Yb^{3+} to Tm^{3+} populate $^3H_5$, $^3F_2$, and $^1G_4$ levels. The $^1D_2$ level of Tm^{3+} cannot be populated by the fourth photon from Yb^{3+} via energy transfer to the $^1G_4$ level due to the large energy mismatch (about 3500 cm^{-1}) between them [13]. The cross-relaxation of $^3F_2 + {}^3H_4 \rightarrow {}^3H_6 + {}^1D_2$ between Tm^{3+} ions may alternatively play an important role in populating $^1D_2$ level [14].

Subsequently, the populated $^1D_2$ level radiatively relaxes to the ground-state and inter-states, which cause 362-, 457-, 510-, and 580-nm emissions, as shown in the inset of Fig. 2. On the other hand, the electron in the $^1D_2$ level may be excited to the $^3P_2$ level via another energy transfer process, produce 265- and 309-nm emissions, simultaneously. In our previous observations [9,13], the $^3P_2$ level usually relaxed to $^1I_6$ level and emitted 291 and 347-nm UV UC fluorescence. Radiative transitions from the $^3P_2$ level are difficult to occur due to the nearby $^3P_{0,1}$ and $^1I_6$ levels offer the routes for rapidly nonradiative relaxation. Of course, the UC emissions from the $^1I_6$ are still dominating in the five-photon UC processes due to the rapidly nonradiative relaxation of $^3P_2 \rightarrow {}^3P_1 \rightarrow {}^3P_0 \rightarrow {}^1I_6$. For a relative high doping concentration, the microcrystals therefore emitted intense 347- and 291-nm fluorescence under the 980-nm excitation.

In comparison with those from the Yb^{3+}/Tm^{3+}-codoped YF_3 nanobundles reported previously [17], the UV emissions from the octahedral nanocrystals are greatly enhanced. It is well known that the shapes, sizes, crystallinity, and dopant concentrations have great effects on the UC luminescence intensities of nanocrystals [5,17,18]. First, the nanocrystals and nanobundles were synthesized by the same method but with different reagents and at different reaction temperatures. For example, we used NH_4HF_2 for octahedral nanocrystals and NaF for nanobundles. All of these resulted in different shapes, sizes, and crystallinity of samples. Second, in this work, the Tm^{3+} concentration of octahedral nanocrystals was 2 mol%, which are different from the nanobundles reported previously. In our previous paper, the Tm^{3+} concentration was 1 mol%. To study the effect of shapes and sizes of nanocrystals on the UV UC emissions, the YF_3:Yb^{3+}/Tm^{3+} octahedral nanocrystals and nanobundles with the same dopant concentrations were synthesized. Note that previously we also measured the transmission electron microscopy images and XRD patterns of YF_3:Yb^{3+}/Tm^{3+} nanobundles. Each nanobundle consists of numerous nanowhiskers with a mean length of ~700 nm and a mean diameter of ~2 nm [17,19]. The UC luminescence spectra and corresponding SEM images of YF_3:Yb^{3+}(20%)/Tm^{3+}(2%) octahedral nanocrystals and nanobundles are shown in Fig. 5. Obviously, the UV UC emissions from octahedral nanocrystals are much stronger than those from nanobundles. On the one hand, the enhancement of UV UC emissions is closely related to the crystallinity (the half width of the diffraction peak (0 2 0) was determined to be 0.29°), shapes, and sizes of nanocrystals. On the other hand, the average number of adjacent Tm^{3+} ions around certain Tm^{3+} ions in the sample with higher surface area is lower than that in sample with lower surface area. This means that local concentration of Tm^{3+} is smaller in samples with higher surface. The octahedral nanocrystals have lower surface area than the nanobundles, resulting in higher local concentration of Tm^{3+} in octahedral nanocrystals. Furthermore, in comparison with those of the bulk sample having the same chemical compositions, the UV emissions from the nanocrystals were greatly enhanced.

To study the effect of dopant concentrations on the UV UC emissions, the dependence of Tm^{3+} concentrations on the

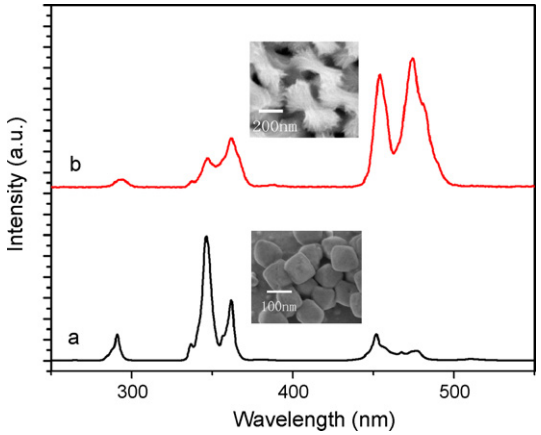

Fig. 5. UC luminescence spectra and corresponding SEM images of YF_3:Yb^{3+}(20%)/Tm^{3+}(2%) nanocrystals (a) and nanobundles (b).

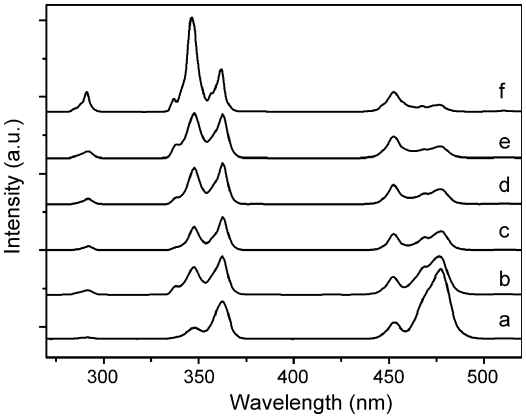

Fig. 6. Dependence of UC emission spectra (normalized to $^1D_2 \rightarrow {}^3F_4$ transition) on Tm^{3+} concentration (20% Yb^{3+}): (a) 0.05%, (b) 0.1%, (c) 0.5%, (d) 1%, (e) 1.5%, and (f) 2%.

fluorescence was studied. The spectra of the $Y_{0.8-y}Yb_{0.2}Tm_yF_3$ (y = 0.0005, 0.001, 0.005, 0.01, 0.015, and 0.02) octahedral nanocrystals are shown in Fig. 6. With the increase of Tm^{3+} concentration, the $^1I_6 \rightarrow {}^3H_6$, $^1I_6 \rightarrow {}^3F_4$, $^1D_2 \rightarrow {}^3H_6$, and $^1D_2 \rightarrow {}^3F_4$ transitions gradually became stronger and predominant over the $^1G_4 \rightarrow {}^3H_6$ transition. When the Tm^{3+} concentration reaches to 2 mol%, the luminescence intensity of $^1I_6 \rightarrow {}^3H_6$ (~291 nm) is ~3 times stronger than that of $^1G_4 \rightarrow {}^3H_6$ (~477 nm). When the Tm^{3+} concentration was higher than 2%, the emissions decreased due to the quenching.

3. Conclusions

Highly uniform and monodisperse YF_3:Yb^{3+}(20%)/Tm^{3+}(2%) octahedral nanocrystals were synthesized through a facile microemulsion method and characterized by XRD and SEM. The nanocrystals emitted weak blue and intense UV light under 980-nm excitation. Especially, the $^3P_2 \rightarrow {}^3H_6$ (~265 nm) and $^3P_2 \rightarrow {}^3F_4$ (~309 nm) emissions were observed. The $^1I_6 \rightarrow {}^3H_6$, $^1I_6 \rightarrow {}^3F_4$, $^1D_2 \rightarrow {}^3H_6$, and $^1D_2 \rightarrow {}^3F_4$ transitions were much stronger than the $^1G_4 \rightarrow {}^3H_6$ transition. Such strong UV UC luminescence has never been observed in other Yb^{3+}/Tm^{3+}-codoped YF_3 nanocrystals.

4. Experimental

Cetyltrimethylammonium bromide (CTAB), cyclohexane, 1-pentanol, ammonium hydrogen fluoride (NH_4HF_2), sodium fluoride (NaF) and hydrochloric acid (HCl) were supplied by Beijing Chemical Reagent Company, and were of analytical grade. Yttrium oxide (Y_2O_3, 99.99%), ytterbia (Yb_2O_3, 99.99%), and thulium oxide (Tm_2O_3, 99.99%) were supplied by Shanghai Chemical Reagent Company. All of the reagents and solvents were used as received without further purification. Deionized water was used to prepare solutions. Y_2O_3, Yb_2O_3, and Tm_2O_3 were separately dissolved in dilute HCl by heating to prepare the stock solutions of YCl_3, $YbCl_3$, and $TmCl_3$.

Two identical solutions, denoted as microemulsion I and II, were prepared by dissolving 2.25 g of CTAB in 50 mL of cyclohexane and 2.5 mL of 1-pentanol. The two microemulsions were stirred separately for 30 min, and then 2 mL of 0.5 M $LnCl_3$ (Ln = Y, Yb, and Tm) aqueous solution and 2 mL of NH_4HF_2 aqueous solution were added dropwise to microemulsion I and II, respectively. After vigorous stirring for 1 h, the two optically transparent microemulsion solutions were mixed and stirred for another 1 h. After aging at 40 °C for 24 h, the emulsion mixture was centrifuged at 12,000 rpm for 10 min, which caused sedimentation of the products and allowed removal of mother liquor. The precipitate was washed thoroughly and dried in vacuum at 80 °C to obtain YF_3:Yb^{3+}/Tm^{3+} octahedral nanocrystals. Nanobundles were prepared by almost the same method but under different reaction conditions. Details of the synthesis have been given in Ref. [17,19]. To improve the crystallinity of the nanocrystals, the products were annealed at 450 °C for 2 h.

Phase identification was performed via X-ray powder diffractometer (Rigaku RU-200b) using a nickel-filtered Cu Kα radiation (λ = 1.4518 Å) in the range of $20^\circ \leq 2\theta \leq 60^\circ$. The size and morphology were investigated by scanning electron microscope (SEM, KYKY 1000B). SEM sample was prepared by placing droplets of the ethanol dispersion on silicon wafer and letting the ethanol evaporate in air. UC luminescence spectra were recorded with a Hitachi F-4500 fluorescence spectrophotometer (2.5 nm for spectral resolution and 400 V for PMT voltage) at room temperature.

Acknowledgment

This research was supported by Natural Science Foundation of China (Grant Nos. 50672030 and 10874058).

References

[1] E. Downing, L. Hesselink, J. Ralston, R. Macfarlane, Science 273 (1996) 1185–1189.
[2] D.A. Parthenopoulos, P. Rentzepis, Science 245 (1989) 843–845.
[3] G. He, J. Dai, T. Lin, P. Markowicz, P. Prasad, Opt. Lett. 28 (2003) 719–721.
[4] S. Sanders, R. Waarts, D. Mehuys, D. Wetch, Appl. Phys. Lett. 67 (1995) 1815–1817.
[5] X. Bai, H. Song, G. Pan, Y. Lei, T. Wang, X. Ren, S. Lu, B. Dong, Q. Dai, L. Fan, J. Phys. Chem. C 111 (2007) 13611–13617.
[6] C. Cao, W. Qin, J. Zhang, Y. Wang, P. Zhu, G. Wei, G. Wang, R. Kin, L. Wang, Opt. Lett. 33 (2008) 857–859.
[7] W. Carnall, R. Fields, K. Rajnank, J. Chem. Phys. 49 (1968) 4424–4442.
[8] M. Hehlen, A. Kuditcher, A. Lenef, H. Ni, Q. Shu, S. Rand, J. Rai, S. Rai, Phys. Rev. B 61 (2000) 1116–1128.
[9] G. Qin, W. Qin, C. Wu, S. Huang, D. Zhao, J. Zhang, S. Lu, Opt. Commun. 242 (2004) 215–219.
[10] J. Qiu, Y. Kawamoto, J. Fluorine Chem. 110 (2001) 175–180.
[11] J. Owen, A. Cheetham, R. Mcfarlane, J. Opt. Soc. Am. B 15 (1998) 684–688.
[12] I. Martin, J. Mendez, V. Rodriguez, J. Romero, J. Garcia, Opt. Mater. 22 (2003) 327–333.
[13] C. Chao, W. Qin, J. Zhang, Y. Wang, P. Zhu, G. Wang, G. Wei, L. Wang, L. Jin, J. Fluorine Chem. 129 (2008) 204–209.
[14] D. Chen, Y. Wang, Y. Yu, P. Huang, Appl. Phys. Lett. 91 (2007) 051920–051922.
[15] M. Pollnau, D. Gamelin, S. Lüthi, H. Güdel, Phys. Rev. B 61 (2000) 3337–3346.
[16] X. Chen, Z. Song, J. Opt. Soc. Am. B 24 (2007) 965–971.
[17] G. Wang, W. Qin, J. Zhang, J. Zhang, Y. Wang, C. Cao, L. Wang, G. Wei, P. Zhu, R. Kim, J. Phys. Chem. C 112 (2008) 12161–12167.
[18] G. Wang, W. Qin, L. Wang, G. Wei, P. Zhu, R. Kim, Opt. Express 16 (2008) 11907–11914.
[19] G. Wang, W. Qin, J. Zhang, J. Zhang, Y. Wang, C. Cao, L. Wang, G. Wei, P. Zhu, R. Kim, J. Fluorine Chem. 129 (2008) 621–624.